RSC Advances

ROYAL SOCIETY OF CHEMISTRY

www.rsc.org/advances

Graphics

The facile and scalable technique is demonstrated, which grow graphene with controllable layers on copper foil substrates using the etching effect of H_2 in atmospheric pressure chemical vapor deposition (APCVD).

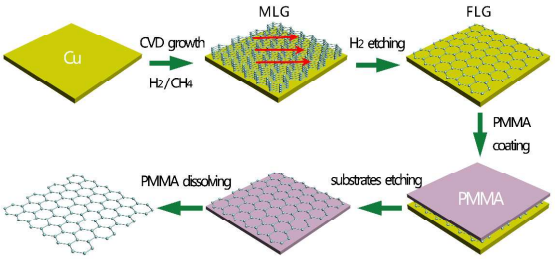

Chemical vapor deposition growth of few-layer graphene for transparent conductive films

Jun Pu,[a] Lei Tang,[a] Chaowei Li,[a] Taotao Li,[a] Lin Ling,[a,b] Kai Zhang,[a] Qingwen Li,[a] and Yagang Yao[*a]

[a] *Key Lab of Nanodevices and Applications, Suzhou Institute of Nanotech and Nanobionics, Chinese Academy of Sciences, University of Chinese Academy of Sciences, 398 Ruoshui Road, Suzhou Industry Park, Suzhou 215123, P. R. China*

[b] *School of Chemical and Material Engineering, Jiangnan University, Wuxi 214122, P. R. China*

[*] Corresponding author. Tel.: 86-512-62872829; Fax: 86-512-62872552; E-mail: ygyao2013@sinano.ac.cn

Abstract

The layer numbers of graphene for graphene based transparent conductive films are crucial. An appropriate number of graphene layers would provide excellent electrical conductivity along with high transparency. Herein, we demonstrated a facile and scalable technique to grow graphene with controllable layers on copper foil substrates using the etching effect of H_2 in atmospheric pressure chemical vapor deposition (APCVD), and studied the influence of H_2 etching on the properties of graphene transparent conductive films. The etching of formed multi-layer graphene (MLG, 12−14 layers) for Cu substrates assists the formation of few-layer graphene (FLG, 2−3 layers). These as-obtained graphene can be used as high performance transparent conductors, which show improved tradeoff between conductivity and transparency: the transmittance of 96.4% at 550 nm with sheet resistance of ~360 Ω sq^{-1}, and the transmittance of 86.7% at 550 nm with sheet resistance of ~142 Ω sq^{-1}. They could be used as high performance transparent conductors in the future.

1. Introduction

Transparent conductive films (TCF) have attracted numerous attentions owing to their high transmittance (in visible light region with λ = 380−780 nm) and excellent electrical conductivity. They are an important part of many optoelectronic devices, such as liquid crystal display (LCD), organic solar cells, organic light emitting diodes (OLED) and electronic touch screens.[1,2] Up to now, indium tin oxide (ITO) is the major material for most of these applications, because of its high transparency, over 90% at 550 nm, and low sheet resistance of 10−30 Ω sq^{-1}.[3] While it is fantastic material, it does have some limitations, including the rising prices of indium, expensive and time-consuming multi-stage process for preparing ITO (spraying and pulsed laser deposition).[4] As a result there has been major interest over the last 15 years in using various forms of nanomaterials for replacing ITO films, such as conductive polymers,[5] metal grids,[6] carbon nanotube,[7] and graphene due to their low sheet resistance and/or high transparency.

Among the numerous ITO alternative materials, graphene is a two-dimensional (2D) nanomaterials of sp^2-hybridized carbon atoms bonded together in a hexagonal lattice, which has many extraordinary properties, such as large specific surface area (~2630 m^2 g^{-1}), large Young's modulus (~1100 GPa), high charge carrier mobility (~200000 cm^2 V s^{-1}), and high thermal conductivity (~5000 W $m^{-1}K^{-1}$).[8−11] The excellent properties in the π-conjugated two-dimensional electron system make graphene a promising candidate for widespread applications in different areas, such as post-silicon electronics,[12] displays,[13] energy storage devices,[14] and sensors.[15]

Therefore, graphene is one of the most potential materials for transparent conductive films due to its optical transparency over a wide range of wavelengths and high electrical conductivity.[16,17] In the past few years, many reports have demonstrated that graphene has the lead in this field.[18,19] Zhang et al. reported that the graphene prepared by chemical vapor deposition (CVD) on tilted copper foil, showed the transmittance of 96.5% at 550 nm with sheet resistance of 600 Ω sq^{-1} (1−3 layers), and the transmittance of 86.7% at 550 nm with sheet resistance of 400 sq^{-1} (5−6 layers). Cheng et al. found an efficient way to make large-area graphene oxide sheets with a sheet resistance of 840 Ω sq^{-1} and 78% transmittance at 550 nm. Despite of these excellent performances, it is flawed because the properties of graphene are very sensitive to its layer numbers.[20] The transmittance increases with superposition of single-layer graphene sequentially, and as a result, as graphene film gets thicker, the transparency is expected to decrease. On the contrary, the sheet resistance of graphene film decreases with the increase of graphene layer.[21,22] For this reason, few-layer graphene (FLG) should have advantages of both high diaphaneity and low resistance together. Therefore, it is highly desirable to synthesize FLG in a large scale to unlock its valuable properties.

A series of approaches to synthesis graphene films have been developed, including mechanical exfoliation, CVD, epitaxial growth, and oxidation-reduction process. Among various graphene synthesis methods, CVD is promising, because it has the capability of making large-scale graphene films with outstanding electrical conductivity and field-effect mobility properties.[23−25] Meanwhile, methane or other

hydrocarbons gas all can be used as carbon source to obtain high quality graphene, which is convenient and feasible.[26] Specially, in high vacuum conditions by controlling the diffusion of carbon species extended monolayer graphene can be achieved with high surface coverage.[27] Unfortunately, the expensive vacuum system may be an inhibiting issue. In general, H_2 seems to serve a dual role in CVD growth of graphene: as a cracking activator of the carbon source on surface; as an etching reagent that controls the size and thickness of the graphene domains.[28] So, how to tune these two kinds of effects of H_2 in order to make FLG with high diaphaneity and low resistance in the CVD process will be a very interesting subject. Skákalová and co-workers synthesized the FLG by CVD on Ni-coated Si substrates under a continuous flow of carrier gases, Ar and H_2, mixed with less than 5 vol.% methane (CH_4:Ar:H_2 = 250:1000:4000 sccm), and they explored the influence of reaction time (30 s and 7 min) on the products during the CVD process.[24] In the present work, we demonstrated an easy strategy to produce FLG (2−3 layers) through etching effects of H_2 in the CVD growth of graphene film on Cu substrate. In addition, more experiment parameters which could affect the final products such as the gas flow rate and etching time were investigated. Such graphene films were transferred by poly(methyl methacrylate) (PMMA) and exhibited good sheet resistance and high transparency in the range of 360 Ω sq^{-1} at 96.4% transparency and 142 Ω sq^{-1} at 86.0% transparency, respectively. We believe that the demonstrated strategy will promote the synthesis of high performance transparent conductive graphene films at large scale and its real applications.

2. Experimental

2.1. Graphene Growth

The 25-μm thick Cu foil with a purity of 99.8 wt % was obtained from Alfa Aesar (No. 13382). Before CVD growth, the Cu foil was pretreatment by hyperacoustic method in acetone and alcohol for 10 min each, and then gently dried with a nitrogen gun. The Cu foil was inserted into a 1.5 inch quartz tube. The temperature was raised to 1000 ºC within 40 min and kept for 30 min in a mixture of H_2 300 standard cubic centimeter per minute (sccm) and Ar 150 sccm. At the beginning of growth process, H_2 flow rate was maintained at 500 sccm, and CH_4 was set at 10 sccm for 3 min to form multi-layer graphene (MLG) (sample No. 1). Then, during the etching process, all gases were switched off, and H_2 of 50 sccm was introduced to the reactor chamber for 30 min to prepare FLG (sample No. 10). Finally, the system was cooled down to room temperature under Ar atmosphere of 150 sccm. In order to study the effects of H_2 and CH_4 on the final graphene product during the additional H_2 exposure process, more detailed experimental procedures and conditions were carried out and summarized in Table S1.

2.2. Graphene Transfer

Graphene grown on Cu surface were transferred onto glass and Si substrates for optical transmittance, electrical conductivity and Raman spectroscopy characterizations by PMMA-assisted transfer method similar to those reported in previous literatures.[19,20] Briefly, a thin PMMA layer (~300 nm) was spin-coated on the

graphene-Cu films at 3000 rpm min^{-1} for 60 s, and then the PMMA-graphene-Cu assembly were baked in oven at 100 ºC for 10 min. In the next step, the ensembles were carefully dipped into aqueous $Fe(NO_3)_3$ solution (1M) for 5 hours. After washing the PMMA-graphene film with deionized water, it was placed onto the target substrates such as Si or glass slide. The final removal of PMMA layer was done by acetone dissolution followed by baking at room temperature.

2.3. Characterization

The samples were characterized by Raman spectroscopy (Raman, Labram HR 800) with laser excitation of 532 nm and Optical micrographs (Nikon A1) at 50× and 100× magnifications, respectively. Scanning electronic microscope (SEM, Hitachi S-4800, 5 KV and 10 KV) was used to observe the morphology of graphene. The tighresolution transmission electron microscopy (HRTEM) and selected area electron diffraction (SAED) images were recorded on a FEI Tecnai G2 20 high-resolution transmission electron microscope performed at an acceleration voltage of 200 kV. X-ray photoelectron spectroscopy (XPS) was recorded on an ESCALab MKII X-ray photoelectron spectrometer with nonmonochromatized Mg Kα X-ray as the excitation source. The optical transmittance of graphene films with an area of 1 × 1 cm^2 on glass was measured by an UV-Vis spectrometer (Perkin Elmer Lambda 25), and the sheet resistance was measured by a four-probe setup with a ST-2258A sourcemeter.

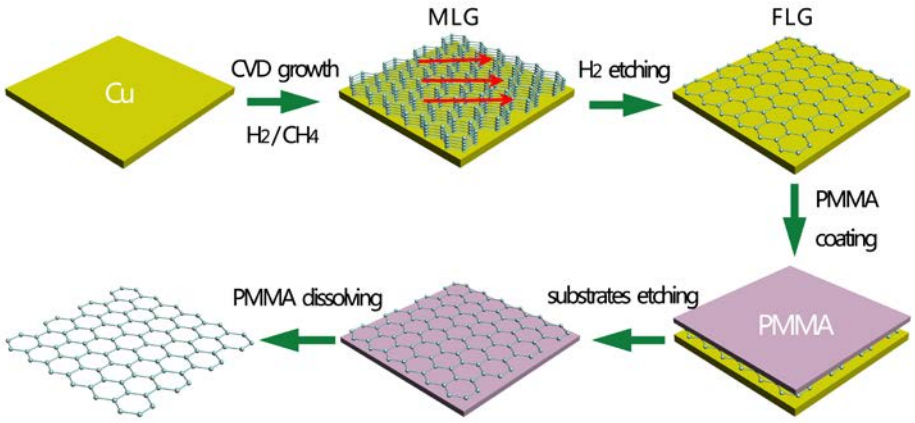

Fig. 1 Schematic illustration for the synthesis, etching, and transfer of graphene films.

3. Results and discussion

Fig. 1 shows the schematic diagram of the easy, feasible CVD strategy for FLG growth. Firstly, metal foils are annealed inside a quartz tube furnace (1.5 inch) under argon and H_2. Through annealing, remaining organic residues on copper surface are removed and at the same time the reduction of the metal films is expected. Secondly, the CH_4 gas introduced into the furnace will be catalytically decomposed into small carbon species. Then these carbon species are incorporated into the Cu substrates at 1000 ºC, and form MLG.[29] Thirdly, after cutting off the carbon supply, the H_2 etching process is performed to etch the MLG for thinning the layers. What's more, it will eliminate the excessive dissolved carbon species.[30,31] Finally, FLG is achieved on Cu substrates. After these steps, through PMMA-assisted method, the grown graphene on Cu surface is also transferred to glass and Si substrates for further characterization.

Optical micrographs of Cu surface after 30 min annealing and the as-prepared FLG (sample No. 10) are shown in Figs. 2a and 2b. It is clearly seen that the Cu surface is smooth through 30 min annealing at 1000 ºC. After growth and etching processes, Cu

substrate was covered with FLG thin film. Fig. 2c shows the SEM image of MLG without the etching section (sample No. 1: H_2 500 sccm, CH_4 10 sccm for 10 min growth). Hexagonal graphene grows uniformly across the growth substrate. There are many dense carbon dots by observing carefully, which may be the nucleation point for graphene.[32] In this CVD period, H_2 could in-diffuse into the Cu substrate and compete with CH_4 for chemisorption. Besides, the H_2 can also passivate defects and grain boundaries.[33,34] After the additional etching process (H_2 50 sccm for 30 min), it can be seen that the density of these carbon dots decreased, indicating that H_2 also etched the carbon points. Fig. 2d and 2e reveal the typical SEM of inceptive hexagon-shaped graphene grown on Cu substrate under the condition of etching with H_2 50 sccm for 30 min. The size of FLG structure is around 3 μm with good uniformity. A higher magnification SEM image in inset of Fig. 2e displays a wrinkled structure on the graphene surface, which most likely arises from the different thermal expansion coefficients between copper and graphene.[3,35] The hexagon edges appear as straight lines and the angles between adjacent edges are all 120°. Fig. 2f shows the typical Raman spectra of these two samples of graphene grown on Cu (sample No. 1 and 10). All grey flakes showed single layer characteristics of graphene, characterized by two peaks located around 2686−2700 cm^{-1} and 1581 cm^{-1}, which reveal that MLG was transformed to FLG by H_2 etching for 30 min. The as-prepared MLG and FLG were further characterized by HRTEM, and the resulting images are displayed in Fig. 2g, and 2h, respectively. Obviously, the layer number of the MLG sample was confirmed to be around 12 to 14 layers, whereas the FLG was comprised of 2 to 3 layers. The

inset of Fig. 2g shows the SAED of MLG. It can be seen that the multideck graphene film demonstrates weak two-dimensional hexagonal packing due to the superposition of many single layer graphene. On the contrary, the SAED result of 2–3 L graphene exhibits a disordered AB stacking between layers (inset of Fig. 2h).

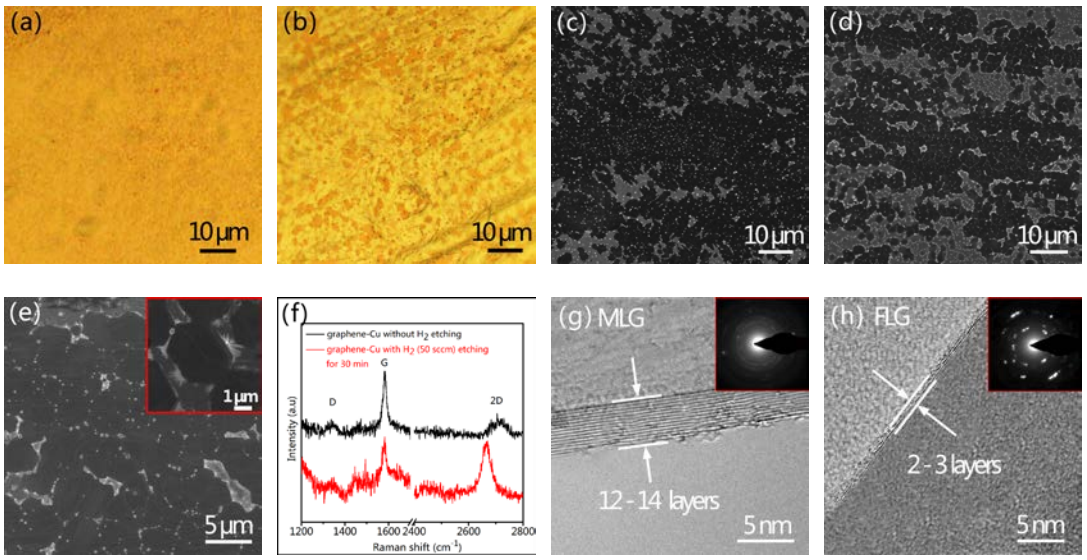

Fig. 2 (a) Optical micrograph of Cu surface after 30 min annealing; (b) Optical micrograph of FLG surface (sample No. 10); (c) SEM image of the MLG (sample No. 1); (d) and (e) SEM images of the sample No. 10 of etched graphene with different magnification, and the inset in e is a high magnification image; (f) Raman spectroscopy of the as-prepared graphene-Cu with and without etching process. (g) HRTEM image of MLG, and the inset is corresponding SAED. (h) HRTEM image of FLG sample, and the inset is corresponding SAED.

In order to explore the etching time effect, the evolution of the G/2D intensity ratio is monitored by varying the etching time from 0 to 90 min under the same conditions

(H_2 50 sccm), which shown in Table S1 (the samples from No. 1 to No. 13). According to the spectrum diagrams in Fig. S1, it can be seen that a lower intensity ratio of G/2D is observed with the extension of etching time.

The amount of H_2 in the etching process also plays an important role on the final graphene products. The SEM results display in Fig. 3 are that the samples prepared by additional etching with 80 and 100 sccm H_2 for 30 min. Careful analysis of these images reveals an important fact that both average size and density of etched area monotonically increase with time, indicating the deterioration of H_2 etching. The inset in Fig. 3b shows typical individual etched pattern obtained at large flow rate of H_2. In this stage, etching starts from the edge of the hexagon (the large white area), and then gradually spread to the center. Thus the graphene become like snowflake (the small white and dark area), and the snowflake-like sample finally disappear as time extends. This observation is consistent with previous literatures.[36,37]

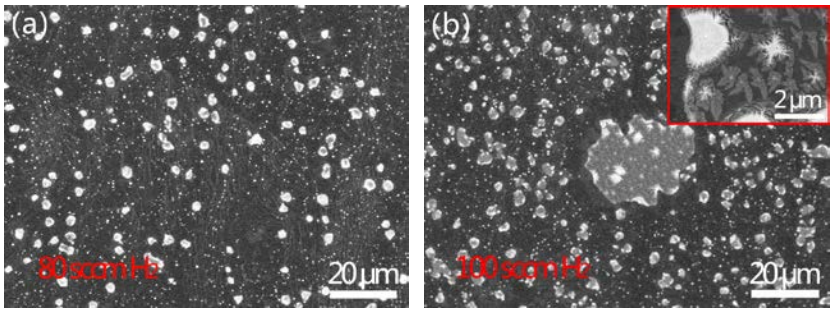

Fig. 3 The SEM images of graphene after etching for 30 min under 80 sccm H_2 and 100 sccm H_2. The inset in b shows typical etched pattern.

In addition, a little amount of CH_4 was introduced in the additional etching step to

weaken the H_2 etching for obtaining high uniformity FLG. Thus, a series of experiments was carried out with various H_2/CH_4 flow rate ratios in the etching process to optimize the amount of introduced CH_4 and the total etching time (the samples from No. 14 to No. 30, see Table S1). More continuous films were prepared as shown in Fig. S2 with the existence of 0.2 sccm CH_4 during the etching process, but the Raman spectra show that these graphene (sample No. 16−18) were multi-layer, though the G/2D intensity ratio is decreasing with the increase of the etching time. Small amount of etching area appeared at the etching time of 60 min and the inset of Fig. S2c shows a high magnification SEM image of one part of the etched area. It was found its shape was different with the snowflake morphology observed above, which was most likely due to the presence of CH_4. Afterwards, the H_2 amount was increased in order to achieve FLG. Graphene samples from No. 19 to No. 21 were synthesized with higher flow rate of H_2 (80, 100, and 150 sccm). As shown in Fig. S3, with the increase of flow rate of H_2, the average size and density of etched graphene (white area) on Cu surface increased as well, proving the corrosion ability of H_2 is stronger. When flow rate of H_2 was increased to 150 sccm, FLG was achieved as Raman spectra proved in Fig. S3d, revealing that with the increase of H_2, etching effect becomes more obvious. However, the graphene film obtained by high H_2 etching became discontinuous due to the larger etched area as shown in Fig. S3c, which is unfavorable for graphene's applications. In the case of samples from No. 22 to No.27 with increasing the CH_4 amount while keeping the H_2 amount at 50 sccm, the Raman results show that when increasing the CH_4 to 0.4 or 1 sccm, no matter how longer the

etching time is (30, 60 or 90 min), the as-obtained graphene were all multi-layer.

Furthermore, we also tried to lower the growth time in the first CVD process while keeping the H_2 amount of 50 sccm in the etching process (samples from No. 28 to No. 30) to thin the layers of graphene. However, we were not able to achieve continuous FLG. It can be clearly seen from the SEM and Raman results shown in Fig. S5 that the density of etched area is larger, which is not beneficial for transparent conductive films. When the etching time was increased to 90 min, the graphene were completely etched away (Fig. S5c), confirming the existence of the H_2 etching effect.

High-quality FLG and MLG synthesized above allow us to investigate graphene's potential application as transparent conductive films. After transferring FLG to glass or Si substrates by PMMA-assisted method, Raman spectroscopy was used to characterize the quality and thickness of the as-transferred graphene samples of FLG (sample No. 10) and MLG (sample No. 1) . The results are revealed in Fig. 4. Graphene has two typical Raman characteristics peaks, G band at about 1580 cm^{-1} and 2D band at about 2670 cm^{-1}, which belong to the in-plane vibrational mode and the intervalley double resonance scattering around the K-point of the Brillouin zone, respectively.[38–40] In addition, there are other two defects induced peaks at about 1340 and 1620 cm^{-1} in obtained Raman curves. Defects through an intervalley double-resonance Raman process activated the D band (1340 cm^{-1}). While the D' band (1620 cm^{-1}) is assigned to the intravalley double-resonance process.[35] The Raman spectrum of as-transferred FLG in Fig. 4a shows lower D peak, sharper G peak, higher and more intense 2D peak, and a lower G/2D intensity ratio (0.8) than

that of MLG without the H_2 etching process. These features are consistent with previous reports, indicating that the sample is FLG and MLG, respectively.[41–43] Fig. 4b reveals the local Raman data of 2D peak position. With the increase of graphene layers, half peak width of 2D peak increases, and it also has a blue shift phenomenon, which agree with the results in Fig. 2f. In this figure, the 2D peak shifts from 2681.7 cm^{-1} to 2690.6 cm^{-1}, which confirms that during the additional period of H_2 exposure, MLG was transformed to FLG by H_2 etching.

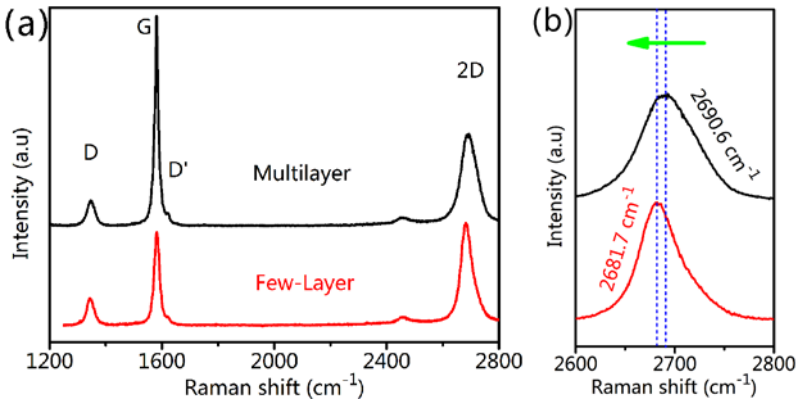

Fig. 4 Raman spectroscopy of the as-transferred MLG and FLG: (a) typical survey spectra; (b) Raman data of 2D peak position.

The functional groups and electronic state of the elements of graphene were determined using the XPS technique. The XPS results of N element of graphene before and after transfer are shown in Fig. S6. Only a little bit of N elements are obtained, and these N are generated from residual PMMA or the doping from $Fe(NO_3)_3$. Fig. 5 proves the C 1s core level spectrum of graphene before and after transfer. The C 1s spectra can be divided into a C=C peak at 284.6 V and a C-C bond

at 285.1 V, assigned to C sp^2 and C sp^3 bonds, respectively. This phenomenon may be due to the existence of both amorphous graphitic carbon and defects.[44,45] However, the distinction of the two XPS spectra is that the spectrum of transferred graphene includes two other chemical bonds (286.5 V and 289.1 V), which are associated with the bonding of carbon atoms in polymer backbone and the methoxy function group, probably because of the PMMA residues on the graphene surface inevitably.[46]

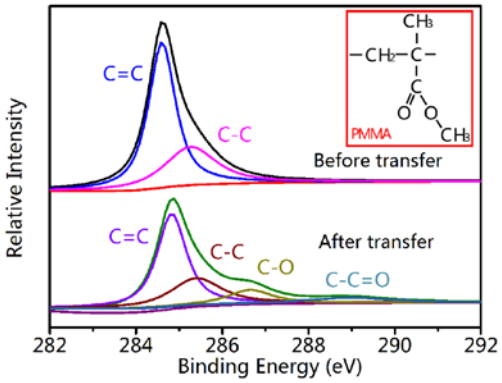

Fig. 5 High-resolution XPS scan for the C 1s core level peak of the as-transferred FLG.

The quality of graphene after transfer is a major concern when it is intended for use in transparent conductive electrode-based applications.[47] UV-Vis spectrometer and four-probe sourcemeter were used to characterize the transmittance and sheet resistance. Uv-vis spectra exhibit the diaphaneity of as-prepared graphene films as wavelength of the incident light with a blank coverslip used for background subtraction (see Fig. 6a). It can be seen that transmittance of graphene in high band region is high, and goes down with the decrease of the band. At 550 nm, the

as-obtained FLG film exhibits a high transmittance of 96.4%, higher than primitive MLG without H_2 etching (89.6%), further indicating that the luminousness of graphene films could be improved by creating the additional stage of H_2 etching to thin the graphene layers. The sheet resistances for MLG and FLG are 142 and 360 Ω sq^{-1}, respectively. Fig. 6b presents a comparison of transparent conductor performances (sheet resistance and transmittance) of as-grown graphene films with previously reported graphene films. Our results show a significant increase in tradeoff between conductivity and transparency, which indicates that as-grown graphene can be used as transparent conductors, and also prove H_2 etching of graphene layers. The as-obtained graphene exhibit a better property compared with the previous reports by Zhang et al. (transparency of 86.7−96.5%, and sheet resistance of 400−600 Ω sq^{-1}),[18] Ahn et al. (transparency of 80−95%, and sheet resistance of 510−280 Ω sq^{-1}).[41] and Rodney S. Ruoff et al. (transparency of 93−97%, and sheet resistance of 350−980 Ω sq^{-1}).[48] However, our results were poorer than these reports by Lee (transparency of 97.7%, and sheet resistance of 210 Ω sq^{-1}) and Bae (transparency of 90.1−97.4%, and sheet resistance of 30−145Ω sq^{-1}),[49,50] revealing that there is still a room for improving the quality of the graphene grown by CVD for use in transparent conducting electrode applications.

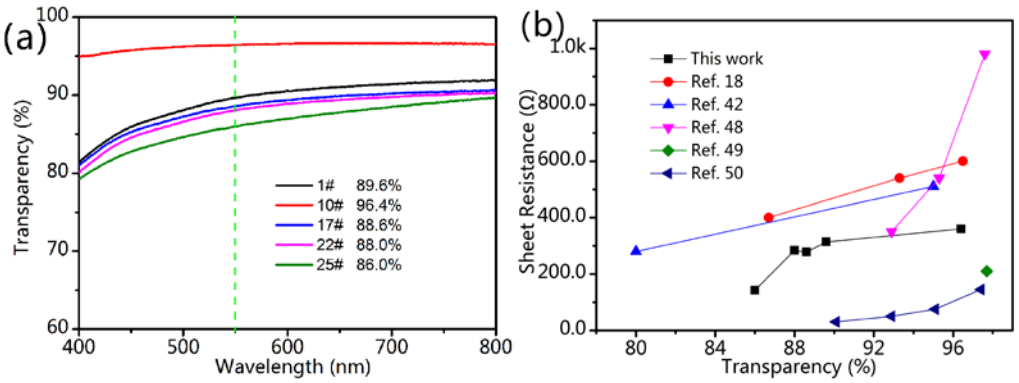

Fig. 6 (a) The transmittance curves of graphene films transferred on glass substrate (sample No. 1, No. 10, No. 17, No. 22 and No. 25); (b) Comparison of sheet resistance versus light transmittance at 550 nm.

Fig. 6b shows the sheet resistance as a function of the optical transmittance. As shown in this curve, the electrical conductivity and light transmittance present a inversely proportional relationship, where the relationship between sheet resistance and transmittance generally agree with the Beer-Lambert rule.[47,51] According to the Beer-Lambert law, the transmittance of light (T) through a homogeneous material can be obtained from the following equation:

$$T = e^{-\alpha d} \quad (1)$$

where d is the thickness of graphene film, and α is the effective absorption coefficient evaluated by $R = 4\pi k/\lambda$, k is the extinction coefficient, and λ is the wavelength of incident light. While, the sheet resistance is defined as this equation:

$$R = \frac{1}{Gd} \quad (2)$$

where G is the material conductivity, and d is the thickness. The electrical conductivity of 2D graphene can be obtained from $\sigma = ne\mu$, where n is the carrier

density, e is the elementary charge, and μ is the mobility. Combining these two equations yields:

$$R = \frac{-4\pi k}{G\lambda \ln T} \quad (3)$$

where k is about of 1.4 for graphene at 550 nm.[52] Deducing from the formula (3), it can be found that the results of transmittance and sheet resistance for as-prepared graphene matched the relationship.

In general, it can be used in real life as long as the square resistance of transparent conductive film is less than 300 Ω and transparent rate is higher than 85%. Therefore, the results present a significant improvement of conductivity and transparency, demonstrating that as-developed method of FLG preparation can replace ITO as a new generation of transparent conductive films for optoelectronic devices in the future.

4. Conclusion

In summary, we systematically investigated the effects of CVD growing and H_2 etching on CVD synthesis of graphene. Based on these effects, we developed an easy and scalable technique for the growth of high-quality FLG on Cu foil by intruding an additional H_2 etching after the growth of MLG. In the additional etching stage, appropriate amount of H_2 and proper etching time are preferred to generate FLG. These controllable graphenes can be used as high performance transparent conductors with transparency of 86.0−96.4%, and sheet resistance of 142−360 Ω sq^{-1}. This research provides a new direction to prepare controllable graphene. In principle, the

approach is not only applicable for FLG growth on copper substrate, but also can be extended to other functional carbon materials and processes possible by CVD on industrial scale.

Acknowledgements

This work was supported by Natural National Science Foundation of China (No. 51372265), the Natural Science Foundation of Jiangsu Province, China (No. BK20140392), and the Science and Technology Project of Suzhou, China (No. ZXG201428 and No. ZXG201401).

References

1. L. B. Hu, D. S. Hecht and G. Grüner, *Chem. Rev*., 2010, **10**, 5790−5844.
2. J. H. Du, S. F. Pei, L. P. Ma and H. M. Cheng, *Adv. Mater*., 2014, **26**, 1958−1991.
3. J. Heo, A. S. Hock and R. G. Gordon, *Chem. Mater*., 2010, **22**, 4964−4973.
4. Z. Chen, B. Cotterell, W. Wang, E. Guenther and S. J. Chua, *Thin Solid Films*, 2001, **394**, 201−206.
5. A. Patra, Y. H. Wijsboom, S. S. Zade, M. Li, Y. Sheynin, G. Leitus and M. Bendikov, *J. Am. Chem. Soc*., 2008, **130**, 6734−6736.
6. M. G. Kang, M. S. Kim, J. Kim and L. J. Guo, *Adv. Mater*., 2008, **20**, 4408−4413.
7. F. C. Meng, X. H. Zhang, G. Xu, Z. Z. Yong, H. Y. Chen, M. H. Chen, Q. W. Li and Y. T. Zhu, *ACS Appl. Mater. Interfaces*, 2011, **3**, 658−661.
8. M. D. Stoller, S. Park, Y. Zhu, J. An and R. S. Ruoff, *Nano Lett*., 2008, **8**, 3498−3502.
9. C. Lee, X. Wei, J. W. Kysar and J. Hone, *Science*, 2008, **321**, 385−388.
10. D. Yuvaraj, K. N. Rao and K. Barai, *Solid State Commun*., 2009, **149**, 349−351.
11. A. A. Balandin, S. Ghosh, W. Bao, I. Calizo, D. Teweldebrhan, F. Miao and N. L. Chun, *Nano Lett*., 2008, **8**, 902−907.
12. Y. M. Lin, K. A. Jenkins, G. A. Valdes, J. P. Small, D. B. Farmer and P. Avouris, *Nano Lett*., 2009, **9**, 422−426.
13. L. Q. Wu, W. W. Li, P. Li, S. T. Liao, S. Q. Qiu, M. L. Chen, Y. F. Guo, Q. Li, C. Zhu, and L. W. Liu, *Small*, 2014, **10**, 1421−1429.
14. B. Wu, D. C. Geng, Y. L. Guo, L. P. Huang, Y. Z. Xue, J. Zheng, J. Y. Chen, G.

Yu, Y. Q. Liu, L. Jiang and W. P. Hu, *Adv. Mater*., 2011, **23**, 3522−3525.

15. B. Huang, Z. Y. Li, Z. R. Liu, G. Zhou, S. G. Hao, J. Wu, B. L. Gu and W. H. Duan, *J. Phys. Chem. C*, 2008, **112**, 13442−13446.

16. K. Rana, J. Singh and J. H. Ahn, *J. Mater. Chem. C*, 2014, **2**, 2646−2656.

17. S. De and J. N. Coleman, *ACS Nano*, 2010, **4**, 2713−2720.

18. J. Zhang, P. A. Hu, X. N. Wang, Z. L. Wang, D. Q. Liu, B. Yang and W. W. Cao, *J. Mater. Chem*., 2012, **22**, 18283−18290.

19. J. P. Zhao, S. F. Pei, W. C. Ren, L. B. Gao and H. M. Cheng, *ACS Nano*, 2010, **4**, 5245−5252.

20. B. Partoens and F. M. Peeters, *Phys. Rev. B*, 2006, **74**, 075404.

21. L. G. D. Arco, Y. Zhang, C. W. Schlenker, K. Ryu, M. E. Thompson and C. W. Zhou, *ACS nano*, 2010, **4**, 2865−2873.

22. X. S. Li, Y. W. Zhu, W. W. Cai, M. Borysiak, B. Y. Han, D. Chen, R. D. Piner, L. Colombo and R. S. Ruoff, *Nano Lett*., 2009, **9**, 4359−4363.

23. W. H. Lee, J. Park, S. H. Sim, S. Lim, K. S. Kim, B. H. Hong and K. Cho, *J. Am. Chem. Soc*., 2011, **133**, 4447−4454.

24. H. J. Park, J. B. Meyer, S. Roth and V Skákalová, *Carbon*, 2010, **48**, 1088−1094.

25. M. Choucair, P. Thordarson, J. A. Stride, *Nature Nanotech.*, 2009, **4**, 30−33.

26. X. S. Li, W. W. Cai, J. An, S. Kim, J. Nah, D. X. Yang, R. Piner, A. Velamakanni, I. Jung, E. Tutuc, S. K. Banerjee, L. Colombo, R. S. Ruoff, *Science*, 2009, **324**, 1312−1314.

27. M. Xu, D. Fujita, K. Sagisaka, E. Watanabe and N. Hanagata, *ACS Nano*, 2011, **5**, 1522−1528.

28. R. Yang, L. C. Zhang, Y. Wang, Z. W. Shi, D. X. Shi, H. J. Gao, E. G. Wang and G. Y. Zhang, *Adv. Mater*., 2010, **22**, 4014−4019.

29. Y. G. Yao, Z. Li, Z. Lin, K. S. Moon, J. Agar and C. P. Wong, *J. Phys. Chem. C*, 2011, **115**, 5232−5238.

30. L. Zhu, Y. Sun, D. W. Hess and C. P. Wong, *Nano Lett*., 2006, **6**, 243−247.

31. Y. G. Yao, C. Feng, J. Zhang, Z. F. Liu, *Nano Lett*., 2009, **9**, 1673−1677.

32. G. H. Han, F. Gunes, J. J. Bae, E. S. Kim, S. J. Chae, H. J. Shin, J. Y. Choi, D. Pribat and Y. H. Lee, *Nano Lett*., 2011, **11**, 4144−4148.

33. M. Losurdo, M. M. Giangregorio, P. Capezzuto and G. Bruno, *Phys. Chem. Chem. Phys*., 2011, **13**, 20836−20843.

34. I. Vlassiouk, M. Regmi, P. Fulvio, S. Dai, P. Datskos, G. Eres and S. Smirnov, *ACS Nano*, 2011, **5**, 6069−6076.

35. X. H. Cao, Y. M. Shi, W. H. Shi, G. Lu, X. Huang, Q. Y. Yan, Q. C. Zhang and H. Zhang, *Small*, 2011, **7**, 3163−3168.

36. X. R. Wang and H. J. Dai, *Nat. Chem*., 2010, **2**, 661−665.

37. D. C. Geng, B. Wu, Y. L. Guo, B. R. Luo, Y. Z. Xue, J. Y. Chen, G. Yu and Y. Q. Liu, *J. Am. Chem. Soc*., 2013, **135**, 6431−6434.

38. Z. W. Shi, R. Yang, L. C. Zhang, Y. Wang, D. H. Liu, D. X. Shi, E. G. Wang and G. Y. Zhang, *Adv. Mater*., 2011, **23**, 3061−3065.

39. A. C. Ferrari, *Solid State Commun*., 2007, **143**, 47−57.

40. W. X Zhang, J. C. Cui, C. A. Tao, Y. G. Wu, Z. P. Li, L. Ma, Y. Q. Wen, G. T. Li, *Angew. Chem.*, 2009, **121**, 5978−5982.

41. T Kato and R Hatakeyama, *ACS Nano*, 2011, **6**, 8508−8515.

42. Y. Lee, S. Bae, H. Jang, S. Jang, S. E. Zhu, S. H. Sim, Y. Song, B. H. Hong and J. H. Ahn, *Nano Lett*., 2010, **10**, 490−493.

43. L. C. Zhang, M. Ni, D. H. Liu, D. X. Shi and G. Y. Zhang, *J. Phys. Chem. C*, 2012, **116**, 26929−26931.

44. C. Y. Yang, H. Bi, D. Y. Wan, F. Q. Huang, X. M. Xie and M. H. Jiang, *J. Mater. Chem. A*, 2013, **1**, 770−775.

45. D. C. Wei, Y. Q. Liu, H. L. Zhang, L. P. Huang, B. Wu, J. Y. Chen, G. Yu, *J. Am. Chem. Soc*., 2009, **131**, 11147−11154.

46. W. H. Lin, T. H. Chen, J. K. Chang, J. I. Taur, Y. Y. Lo, W. L. Lee, C. S. Chang, W. B. Su and C. I. Wu, *ACS Nano*, 2014, **8**, 1784−1791.

47. Y. Zhu, Z. Z. Sun, Z. Yan, Z. Jin, J. M. Tour, *ACS Nano*, 2011, **5**, 6472−6479.

48. J. W. Suk, A. Kitt, C. W. Magnuson, Y. F. Hao, S. Ahmed, J. An, A. K. Swan, B. B. Goldberg and R. S. Ruoff, *ACS Nano*, 2011, **5**, 6916−6924.

49. D. M. Lee, G. D. Kwon, J. H. Kim, E. Moyen, Y. H. Lee, S. Baik and D. Pribat, *Nanoscale*, 2014, **6**, 12943−12951.

50. S. K. Bae, H. K. Kim, Y. Lee, X. F. Xu, J. S. Park, Y. Zheng, J. Balakrishnan, L. Tian, H. R. Kim, Y. Song, Y. J. Kim, K. S. Kim, B. Özyilmaz, J. H. Ahn, B. H. Hong and S. Iijima, *Nat. Nanotechnol*., 2010, **5**, 574−578.

51. W. W. Cai, Y. W. Zhu, X. S. Li, R. D. Piner and R. S. Ruoff. *Appl. Phys. Lett*.,

2009, **95**, 123115.

52. A. Gray, M. Balooch, S. Allegret, G. S. De and W. E. Wang, *J. Appl. Phys.*, 2008, **104**, 053109.